SCIENTIFIC REPORTS

OPEN

Correspondence and requests for materials should be addressed to S.H. (shinjih@med. osaka-cu.ac.jp)

* These authors contributed equally to this work.

Post-natal treatment by a blood-brain-barrier permeable calpain inhibitor, SNJ1945 rescued defective function in lissencephaly

Shiori Toba[1]*, Yasuhisa Tamura[2]*, Kanako Kumamoto[1]*, Masami Yamada[1], Keizo Takao[3,4], Satoko Hattori[3,5], Tsuyoshi Miyakawa[3,4,5], Yosky Kataoka[2], Mitsuyoshi Azuma[6], Kiyoshi Hayasaka[7], Masano Amamoto[8], Keiko Tominaga[9], Anthony Wynshaw-Boris[10], Hideki Wanibuchi[11], Yuichiro Oka[12,13,14], Makoto Sato[12,13,14], Mitsuhiro Kato[7] & Shinji Hirotsune[1]

[1]Department of Genetic Disease Research, Osaka City University Graduate School of Medicine, Asahi-machi 1-4-3 Abeno, Osaka 545-8586, Japan, [2]Cellular Function Imaging Laboratory, RIKEN Center for Molecular Imaging Science, Minatojima minamimachi, Chuo-ku, Kobe, Hyogo, Japan, [3]Japan Science and Technology Agency, CREST, 4-1-8 Honcho, Kawaguchi, Saitama 332-0012, Japan, [4]Section of Behavior Patterns, Center for Genetic Analysis of Behavior National Institute for Physiological Sciences, 38 Nishigonaka Myodaiji, Okazaki, Aichi, 444-8585, Japan, [5]Division of Systems Medical Science, Institute for Comprehensive Medical Science, Fujita Health University, Toyoake, Aichi 470-1192, Japan, [6]Senju Laboratory of Ocular Sciences, Senju Pharmaceutical Co., Ltd., 1-5-4, Murotani, Nishi-ku, Kobe, Hyogo 651-2241, Japan, [7]Department of Pediatrics, Yamagata University Faculty of Medicine, Iida-nishi 2-2-2, Yamagata 990-9585, Japan, [8]Pediatric Emergency Center, Kitakyuusyu City Yahata Hospital. Nishimotomachi 4-18-1, Yahatahigasi Kitakyuusyu City, Japan, [9]Department of Internal Medicine, Tokyo Metropolitan Fuchu Medical Center for the Disabled. Musashidai, Fuchu-shi, Tokyo, Japan, [10]Department of Pediatrics and Institute for Human Genetics, University of California, San Francisco, School of Medicine, San Francisco, CA 94143-0794, [11]Department of Pathology, Osaka City University Graduate School of Medicine, Asahi-machi 1-4-3 Abeno, Osaka 545-8586, Japan, [12]Division of Cell Biology and Neuroscience, Department of Morphological and Physiological Sciences, Faculty of Medical Sciences, University of Fukui, [13]Research Center for Child Mental Development, University of Fukui, [14]Research and Education Program for Life Science, University of Fukui.

Toward a therapeutic intervention of lissencephaly, we applied a novel calpain inhibitor, SNJ1945. Peri-natal or post-natal treatment with SNJ1945 rescued defective neuronal migration in *Lis1*$^{+/-}$ mice, impaired behavioral performance and improvement of ^{18}F-FDG uptake. Furthermore, SNJ1945 improved the neural circuit formation and retrograde transport of NFG in *Lis1*$^{+/-}$ mice. Thus, SNJ1945 is a potential drug for the treatment of human lissencephaly patients.

LIS1 encodes a protein carrying seven WD repeats[1,2] that was first identified as a non-catalytic subunit of platelet activating factor-acetylhydrolase (Pafah1b1)[3]. Numerous studies to address the molecular function of LIS1 led to the conclusion that LIS1 is essential for the proper regulation of cytoplasmic dynein[4–6]. We previously reported that calpain inhibition rescued defective phenotypes that are observed in *Lis1*$^{+/-}$ mice[7], suggesting that calpain inhibitors are a potential therapy for the treatment of lissencephaly. Here, we applied a novel blood-brain barrier (BBB) permeable calpain inhibitor, SNJ1945 for the treatment of lissencephaly[8–10].

Results

SNJ1945 rescued defective distribution of cytoplasmic dynein and membranous components in the cell and defective migration in *Lis1*$^{+/-}$ neurons. *In vitro* administration of SNJ1945 protected LIS1 from proteolysis, resulting in the augmentation of LIS1 levels in *Lis1*$^{+/-}$ mouse embryonic fibroblast (MEF) cells and leading to rescue of the aberrant distribution of cytoplasmic dynein and intracellular components including mitochondria and β-COP positive vesicles (Supplementary Fig. 1a–e). SNJ1945 also rescued defective distribution of cytoplasmic dynein and membranous components in human fibroblasts from an isolated lissencephaly sequence (ILS) patient, suggesting that SNJ1945 will be similarly effective in the human (Supplementary Fig.

2a–e). In addition, SNJ1945 improved neuronal migration of *Lis1*^{+/−} cerebellar granular neurons (Supplementary Fig. 3). Notably, administration of even large doses did not result in obvious adverse effects on granular neurons (Supplementary Fig. 4). Oral administration of SNJ1945 to pregnant dams resulted in substantial increases of LIS1 levels in the brain of fetuses, as did oral administration directly to peri-natal offspring or adults (Fig. 1). Importantly, LIS1 levels increased in the brain three weeks after birth (Fig. 1c, f), indicating that indeed SNJ1945 passed through the BBB and inhibited proteolytic degradation of LIS1. Quantitative determination of drug concentrations in tissue homogenates via liquid chromatography-tandem mass spectrometry (LC-MS/MS) is commonly conducted using the standards. We measured the concentration of SNJ1945 in the brain using LC-MS/MS (Supplementary table 1). LC-MS/MS analysis indicated the brain distribution of SNJ 1945.

To demonstrate whether there was therapeutic benefit *in vivo*, we designed four different administration approaches (Fig. 2a): (1) intra-peritoneal injection starting at E9.5 (100 µg/g) followed by oral
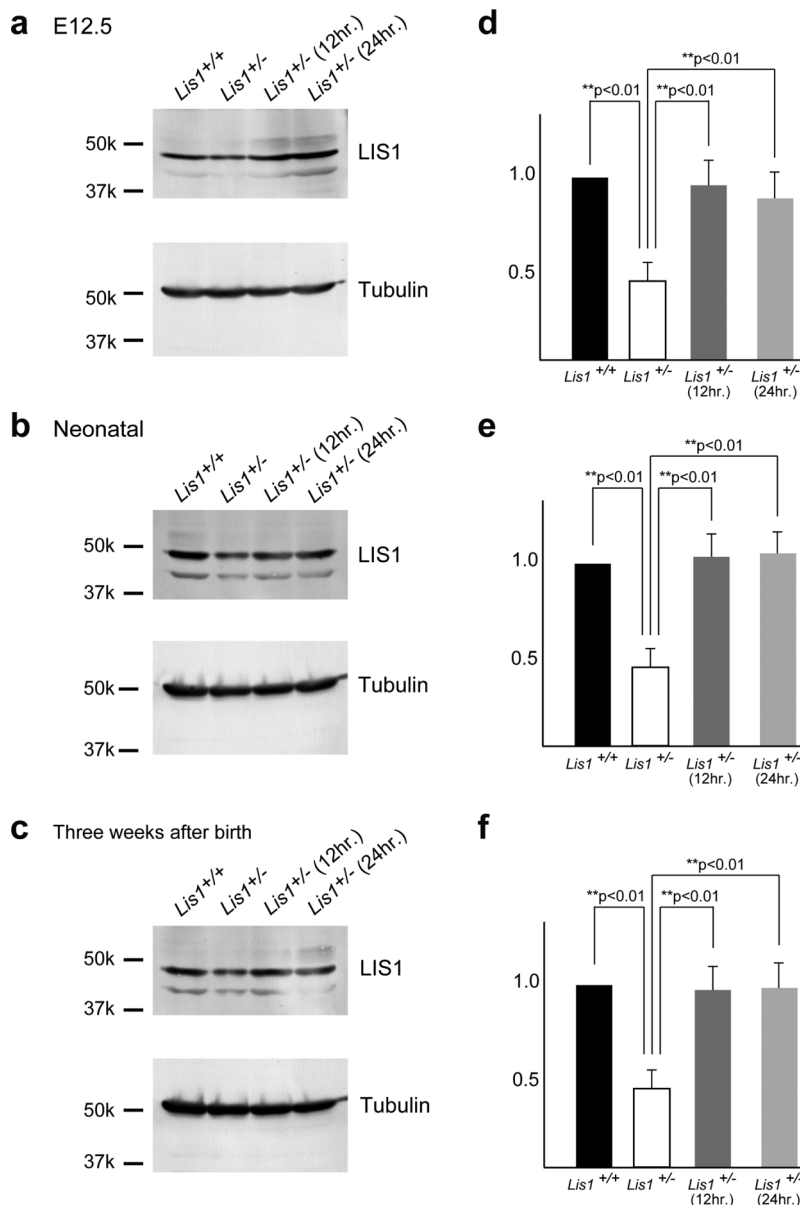

Figure 1 | Rescue of defective corticogenesis in *Lis1*^{+/−} mice by SNJ1945. (a, b, c) Western blotting analysis of the brain after treatment of SNJ1945. Western blotting was performed on brain lysates after oral administration of SNJ1945. Time after oral administration is indicated at the top. Antibodies used for Western blots are indicated at the right of the Western blotting panels. Size maker and each molecular weight were shown at the left. Protein levels were normalized to tubulin beta-3 (Tubulin) as a control and are indicated at a graph (d, e, f). Statistical examination was performed by unpaired Student's *t*-test at 12 and 24 hrs after administration compared to *Lis1*^{+/−}, with **$P < 0.01$. Error bars in graphs were expressed as mean ± SEM. (a, d) SNJ1945 was taken orally as a mixture with food by pregnant dams at E12.5 (200 µg/g). At the indicated time, fetal brains were dissected and subjected to Western blotting analysis. We analyzed ten independent fetuses, and obtained reproducible results. One representative data set is shown. (b, e) SNJ1945 was gavage fed orally as a mixture with 0.5% carboxymethyl cellulose to neonatal pups (200 µg/g). At indicated time, brains of neonatal pups were dissected and subjected to Western blotting analysis. We analyzed ten independent pups. (c, f) SNJ1945 was taken orally as a mixture with food by *Lis1*^{+/−} mice at three weeks after birth (200 µg/g). At indicated time, brain was dissected and subjected to Western blotting analysis. We analyzed ten independent mice, and obtained reproducible results. Note: LIS1 levels were increased to normal levels by 12 hrs. after oral administration. Importantly, SNJ1945 was effective in mice at three weeks, indicating that SNJ1945 is able to pass the BBB and protect LIS1 from degradation.
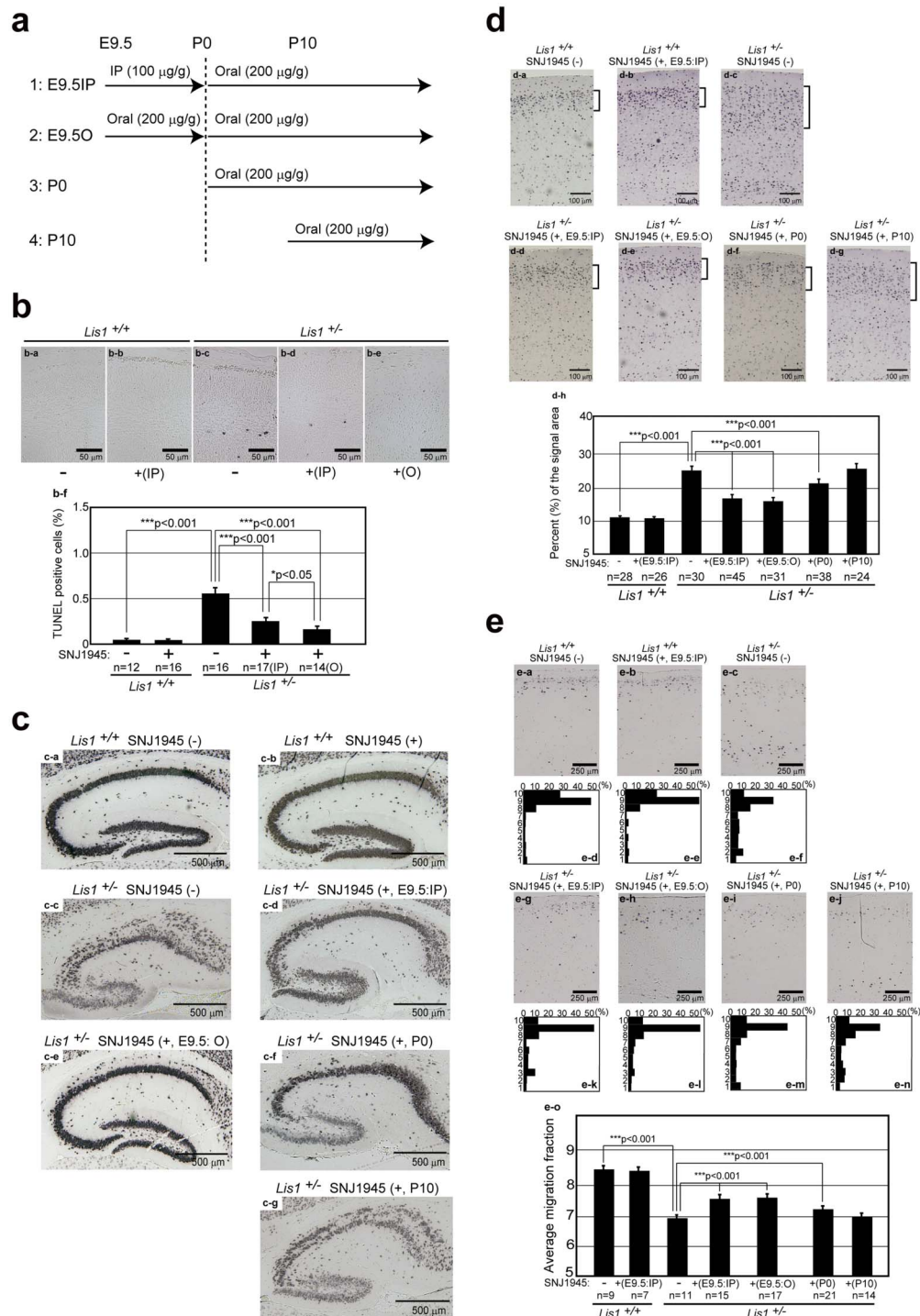
Figure 2 | Rescue of defective corticogenesis in *Lis1*^{+/−} mice by SNJ1945. (a) Administration of SNJ1945 via four protocols (see methods). (b) Apoptotic cell death was examined by TUNEL staining at E15.5. One representative data set is shown (b-a, b, c, d, e). Histogram plots of the relative frequency of TUNEL positive cells to the total number of cells are shown at the bottom (b-f). The staining patterns are representative of different experiments as indicated at the bottom of the panel. *n* is the number of examined brains. Statistical examination was performed by unpaired Student's *t*-test. Error bars in graphs were expressed as mean ± SEM. (c) Neu-N staining of mid-sagittal sections of the hippocampus is shown. Severe cell dispersion and splitting of CA3 region were observed in the *Lis1*^{+/−} mouse hippocampus (c-c), which improved by the administration of SNJ1945 (c-d, e, f, g). Other examples are shown in Supplementary Figure 6. (d) Cortical phenotypes were examined using a layer specific maker, Brn-1 (layer 2 and 3). The distribution of Brn-1 positive cells is indicated at the right side of each panel (d-a, b, c, d, e, f, g). Brn-1 positive cells were more dispersed in the *Lis1*^{+/−} mouse (d-c). Quantitation of the thickness of Brn-1 positive cells is summarized at the bottom (d-h). The staining patterns are representative of different experiments as indicated at the bottom of the panel. The dispersion of Brn-1 positive cells is improved by the administration of SNJ1945. *n* is the number of examined brains. Statistical examination was performed by unpaired Student's *t*-test. Values in graphs were expressed as mean ± SEM. (e) BrdU birthdating analysis revealed neuronal migration defects in the *Lis1*^{+/−} mouse. Quantitation of the thickness of BrdU positive cells is summarized at the bottom (e-o). The distribution of BrdU labeled cells in each bin that was equally divided the cortex from ML to SP. The staining patterns are representative of five different experiments. The shift downward toward the ventricular side as *Lis1* was disrupted. Treatment of SNJ1945 rescued neuronal migration to more superficial (later born and further migrating) areas.

3

administration after birth (200 μg/g), (2) oral administration starting at E9.5 (200 μg/g) followed by oral administration after birth (200 μg/g), (3) oral administration starting in the peri-natal period (200 μg/g) and (4) oral administration starting ten days after birth (200 μg/g). We previously reported a mild reduction of the density of cells in the neocortex of the $Lis1^{+/-}$ mice[11]. At E15.5 when later migrating neurons are generated, a significant acceleration of apoptotic cell death in the ventricular zone was observed[11]. These results prompted us to investigate apoptotic cell death during corticogenesis by TUNEL staining at E15.5 (Fig. 2b). In $Lis1^{+/-}$ mice, apoptotic cell death was clearly increased[11]. In contrast, administration of SNJ1945 suppressed apoptotic cell death in $Lis1^{+/-}$ mice (Fig. 2b). We also examined whether administration of SNJ1945 had any effects on mitotis, since LIS1 is essential for mitotic cell division[12] and neuroepithelial stem cell proliferation[13]. At E13.5, we performed BrdU pulse labeling and found that BrdU incorporation was not significantly different among the five groups (Supplementary Fig. 5), indicating that there was no measureable effect of SNJ1945 on proliferation of neuroepithelial stem cells. We next examined the effect of SNJ1945 on the cortical and hippocampal layering of neurons. $Lis1^{+/-}$ mice exhibited laminar splitting and discontinuities of pyramidal cells in the CA3 and CA2 region of the hippocampus (Fig. 2c), as we previously demonstrated[12]. After administration of SNJ1945 in utero, $Lis1^{+/-}$ mice also displayed splitting and discontinuities in the pyramidal cell layer of the hippocampus, but these defects were markedly improved compared with untreated mice (Fig. 2c and Supplementary Fig. 6a–c). To examine cortical lamination, we analyzed Brn-1 immunoreactivity, to label neurons of layer 2 and 3[14]. In $Lis1^{+/-}$ mice, Brn-1 positive cells (which migrate at later stages) exhibited a broader distribution compared to $Lis1^{+/+}$ mice. Administration of SNJ1945 resulted in more tightly packed layer 2/3 neurons in $Lis1^{+/-}$ mice (Fig. 2d), suggesting that neuronal migration in the cortex was also improved by the inhibition of LIS1 degradation. In both the hippocampus and cortex, oral administration starting postnatally was also partially effective but less effective than when treatment started in utero (Fig. 2c, d and Supplementary Fig. 6a–c). To confirm that the morphological defects observed in $Lis1^{+/-}$ mice were improved by SNJ1945 treatment, we performed quantitative BrdU birthdating analysis. In $Lis1^{+/-}$ mice, the distribution of labeled cells was shifted downward toward the ventricular zone in the cortex, and BrdU-labeling was more diffusely localized (Fig. 2e), as we previously demonstrated[12]. These migration defects associated with the disruption of $Lis1$ were partially rescued in the presence of SNJ1945 (Fig. 2e). Thus, we concluded that oral administration or intra-peritoneal injection of SNJ1945 in utero are effective in rescuing defective neuronal migration. Importantly, oral administration commencing postnatally was also partially effective, resulting in improvement of brains structure including hippocampus and cortex. In contrast, oral administration starting ten days after birth did not result in any obvious benefits, suggesting that some fraction of neurons was still migrating at the time of birth[15], which was essentially complete by ten days after birth.

SNJ 1945 partially rescued impaired motor behavior. $Lis1^{+/-}$ mice displayed abnormal behavior and impaired spatial learning[7,16]. Therefore, we examined whether administration of SNJ1945 to $Lis1^{+/-}$ mice is effective in improving motor behavior compared to untreated $Lis1^{+/-}$ mice. Body weight and temperature were not significantly different among groups, (Supplementary Table 1). As shown in our previous report, $Lis1^{+/-}$ mice exhibited shorter wire-hang latency compared with wild-type mice, and this decreased latency was rescued by SNJ1945 treatment (Fig. 3a). This improvement was most significant in the group in which treatment was started from fetal times ($Lis1^{+/-}$E9.5). Next, we examined rotarod performance. The latency to fall for the SNJ1945-minus group was significantly less than wild type mice, as we previously reported[7]. Impaired

performance on the rotarod test was significantly improved in the SNJ1945-treated groups (Fig. 3b, Supplementary Fig. 7). This functional improvement was also observed not only in the $Lis1^{+/-}$E9.5 group, but also in the $Lis1^{+/-}$P0 group, in which treatment was started perinatally. In our previous report, we demonstrated that in utero treatment of a calpain inhibitor from fetal stages improved gait performance. Consistent with this finding, administration of SNJ-1945 significantly improved the percent of stride in swing and swing to stance ratios in the $Lis1^{+/-}$E9.5 group (Fig. 3c). Most importantly, these improvements were also observed in the $Lis1^{+/-}$P0 and $Lis1^{+/-}$P10 groups. The Porsolt forced swim test is the most commonly used test for assessment of depression-like behavior in animal models. Mice were placed in an inescapable cylinder half-filled with water to induce the behavioral state of despair. We measured periods of immobility, in which longer immobile times indicated higher degrees of despair (Fig. 3d). We found that $Lis1^{+/-}$ mice displayed significantly increased immobile times compared with controls. SNJ1945 treated $Lis1^{+/-}$ groups displayed immobile times intermediate between $Lis1^{+/+}$ mice and $Lis1^{+/-}$ mice. In particular, improvement close to normal levels was observed in the $Lis1^{+/-}$E9.5 group. Our findings suggest that SNJ1945 treatment can rescue depression-like status in $Lis1^{+/-}$ mice. It is possible that the rescue of this behavioral abnormalities in $Lis1^{+/-}$ mice by SNJ1945 treatment results from the improved coordination of motor function by SNJ1945. Another possibility is that treatment of SNJ1945 rescued depression-like status in $Lis1^{+/-}$ mice, which led to improvement of behavioral performance.

Small-animal positron emission tomography (PET) was used for evaluation of brain functional improvement by SNJ1945 treatment. We further addressed whether the rescue of defective behaviors in $Lis1^{+/-}$ mice by SNJ1945 treatment was associated with the improvement of brain function. Small-animal imaging studies using PET have been increasingly applied in murine models for drug discovery[1]. We here employed PET imaging with 2-deoxy-2-^{18}F-fluoro-D-glucose (FDG) to evaluate brain neural activity based on glucose metabolism[17]. We found aberrations in FDG uptake patterns in $Lis1^{+/-}$ mice that responded to SNJ1945 treatment. PET scans with FDG in human lissencephaly patients demonstrated two layers in the cerebral cortex that could be differentiated based on metabolic activity[18], corresponding to the inner cellular layer of the lissencephalic cortex and the molecular, outer cellular, and cell-sparse layers, respectively[18]. In our PET imaging, we were not able to observe such a layered pattern in $Lis1^{+/-}$ mice due to the limitation of spatial resolution (Fig. 4a). $Lis1^{+/-}$ mice displayed similar glucose utilization in the cortex, hippocampus and cerebellum compared to wild type mice (Supplementary Fig. 8). Interestingly, we found significantly reduced glucose utilization in the basal forebrain, hypothalamus and amygdala (Fig. 4a, b). Most importantly, these reductions in FDG uptake were reversed by the treatment with SNJ1945 (Fig. 4a, b). The recovery of glucose metabolism is consistent with the improvement of behavioral performance by treatment with SNJ1945.

SNJ1945 improved neural network formation and facilitated clustering of GABA receptors in amygdala. Because behaviors and brain metabolism are highly linked to the interactive dynamics of neural circuits and synaptic formation in the brain, it is possible that SNJ1945 also rescued defective network formation and synaptogenesis in $Lis1^{+/-}$ mice, which might account for the functional improvement of behavioral performance and FDG uptake even without migratory rescue (such as after treatment commencing at P10). To address this question, we injected $TdTomato$[19] into embryos to visualize neural networks at E16.5[20]. In particular, we have focused on neural networks in amygdala (Fig. 5a). While there were no notable differences in the size of the soma, $Lis1^{+/-}$ mice displayed a striking simplification of dendrites compared to $Lis1^{+/+}$ mice
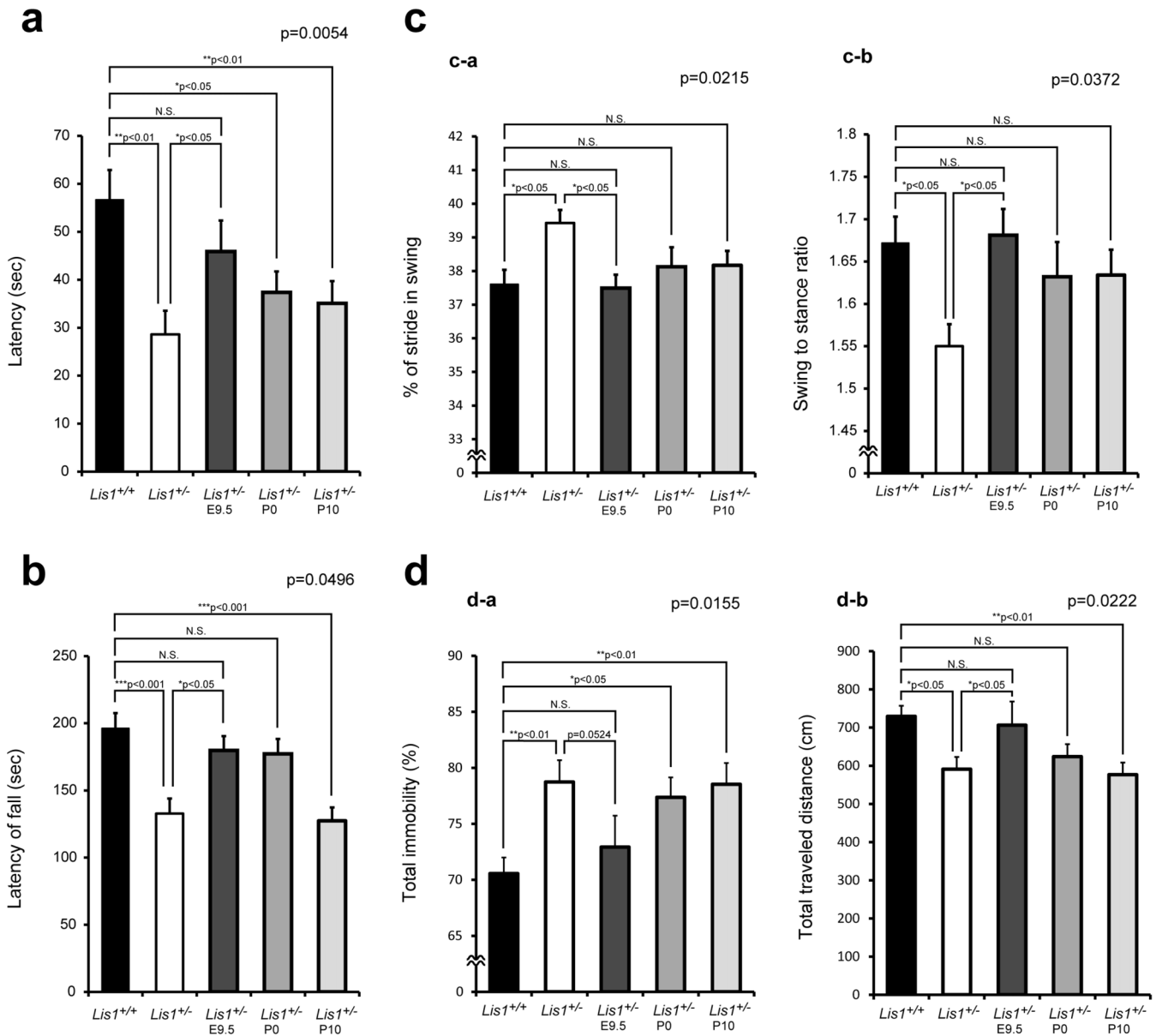
Figure 3 | Mouse behavior analysis. We examined behavioral performance of $Lis1^{+/+}$ mice, $Lis1^{+/-}$ mice and $Lis1^{+/-}$ mice with SNJ1945 treatment after the administration protocol described in Fig. 2a. $Lis1^{+/+}$, wild type mice, $Lis1^{+/-}$; $Lis1^{+/-}$ mice without treatment, $Lis1^{+/-}$E9.5; $Lis1^{+/-}$ mice with oral administration from E9.5 (200 μg/g) followed by oral administration after birth (200 μg/g), $Lis1^{+/-}$P0; $Lis1^{+/-}$ mice with oral administration from peri-natal period (200 μg/g) $Lis1^{+/-}$P10; $Lis1^{+/-}$ mice with oral administration from ten days after birth (200 μg/g). P-values are shown at the upper parts of bars. Statistical analysis was conducted using Stat View (SAS institute). Data were analyzed by one-way ANOVA. Error bars in graphs were expressed as mean ± SEM, and P-values indicated a group effect by one-way ANOVA. Statistical significance was defined as *$P < 0.05$, **$P < 0.01$ and ***$P < 0.001$. (a) Wire hang test. $Lis1^{+/-}$ mice displayed clear shorter latency to fall in the wire hang test. Administration of SNJ1945 improved hanging time. (b) Examination of motor function by the rotarod test. Time spent balanced on top of the rotating rod was measured across six test trials. The graph indicates summation of the latency through the six test trials. Significant differences between $Lis1^{+/+}$ mice and $Lis1^{+/-}$ mice (***$P < 0.001$) were observed. SNJ1945 treatment resulted in improvement of rotarod performance but was less effective with the delayed treatment. Importantly, treatment starting at P0 was still effective. (c) Gait analysis using the DigiGait treadmill apparatus: percent of stride in swing (c-a) and swing to stance ratio (c-b) are shown. $Lis1^{+/-}$ mice with SNJ1945 treatment displayed improvement of gait parameters. Importantly, treatment from P10 was still effective, suggesting SNJ1945 can improve brain function after much of development has finished. (d) Porsolt swimming test. Immobility (d-a) and distance traveled (d-b) are shown at Day 2.

(Fig. 5b, c, d, Supplementary Fig. 9). Branching and length of each branch were decreased to approximately 29% and 27%, respectively. Importantly, the poor development of dendritic arbors and decreased each length in $Lis1^{+/-}$ mice were rescued by SNJ1945 treatment (Fig. 5b, c, d, Supplementary Fig. 9), suggesting that neurons in the amygdala partially maintain plasticity, and proper network formation was facilitated by the treatment after P10.

The amygdala has an important role in processing emotional information[21-23]. Inappropriate processing within the amygdala is thought to induce anxiety disorders. Benzodiazepines, which act specifically on GABA$_A$ receptors, are commonly used as anxiolytics. This implies that GABAergic synapses within the amygdala may have an important role in inducing or compensating for these disorders. GABA$_A$ receptors are clustered at synaptic sites to achieve a
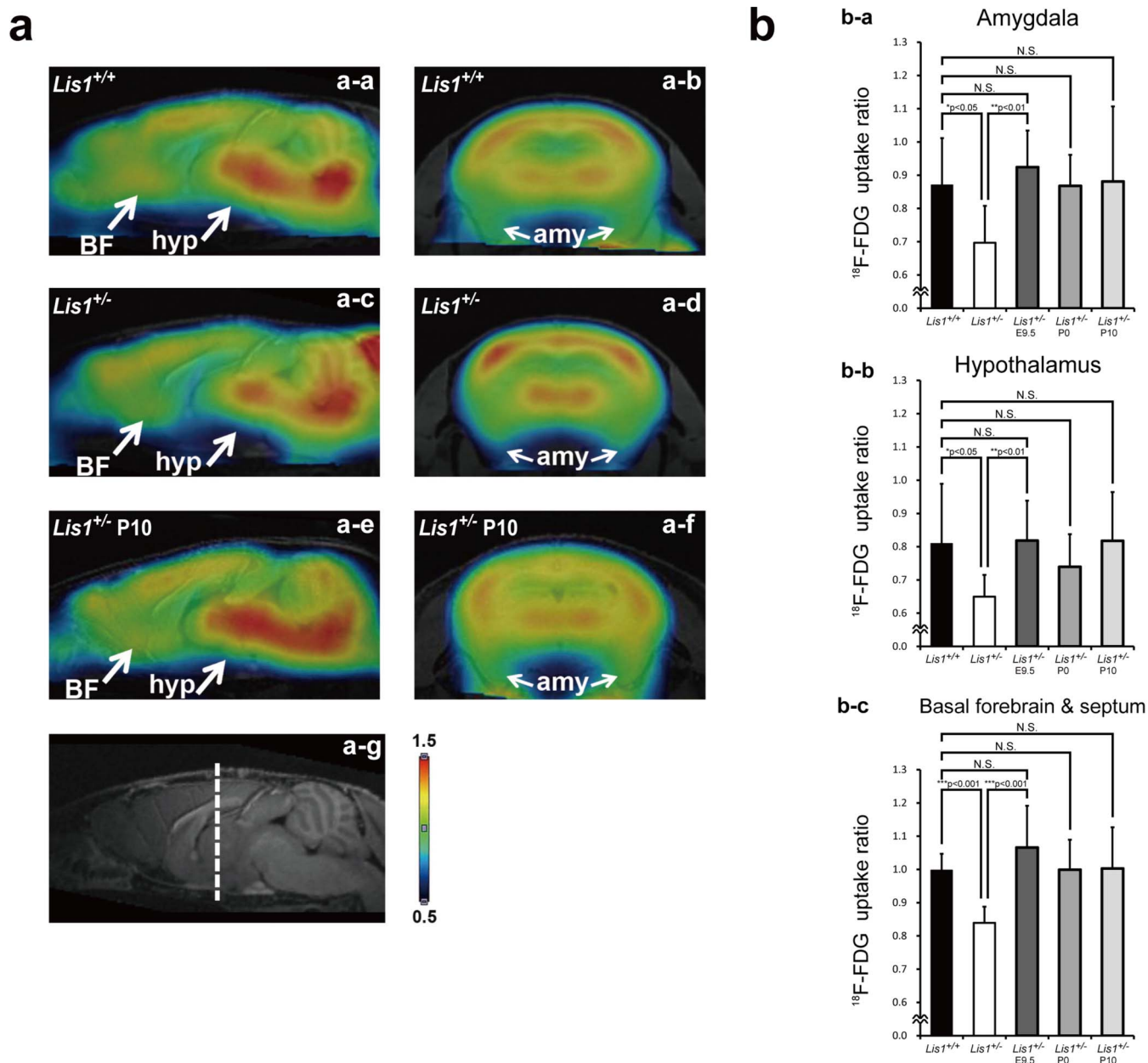
Figure 4 | Brain metabolism: ^{18}F-FDG PET scanning. *In vivo* ^{18}F-FDG-PET images and surface renderings of wild type (WT) mice and *Lis1*$^{+/-}$ mice are depicted. (a) Co-registration of microPET and MRI images obtained from WT mice (a-a, b) or *Lis1*$^{+/-}$ mice (a-c, d, e, f). The basal forebrain and hypothalamus are indicated by white arrows in sagittal images (BF, basal forebrain; hyp, hypothalamus) and amygdala is indicated by white arrows in coronal images (amy, amygdala). The location of coronal slice images is indicated as a white dash line in the sagittal MR image (a-g). Graded 2D slice images demonstrate the reduction of ^{18}F-FDG uptake in the basal forebrain, hypothalamus and amygdala of *Lis1*$^{+/-}$ mice (a-c, d). The color bar indicates normalized ^{18}F-FDG uptake ratio. (b) Quantification of ^{18}F-FDG uptake in several brain regions of each experimental group (*Lis1*$^{+/+}$; *Lis1*$^{+/+}$ mice without treatment (n = 8), *Lis1*$^{+/-}$; *Lis1*$^{+/-}$ mice without treatment (n = 8), *Lis1*$^{+/-}$E9.5; *Lis1*$^{+/-}$ mice with SNJ1945 treatment from E9.5 (n = 6), *Lis1*$^{+/-}$P0; *Lis1*$^{+/-}$ mice with SNJ1945 treatment from peri-natal period (n = 7) *Lis1*$^{+/-}$P10; Lis1$^{+/-}$ mice with SNJ1945 treatment from ten days after birth (n = 6)). Statistical examination was performed by unpaired Student's *t*-test. Values in graphs were expressed as mean ± SEM. Statistical significance was defined as *P < 0.05, **P < 0.01 and ***P < 0.001.

high density of postsynaptic receptors opposite the input axonal terminals. This allows for an efficient propagation of GABA mediated signals, which mostly result in neuronal inhibition. A key organizer for GABA$_A$ receptors is gephyrin that forms oligomeric superstructures beneath the synaptic area[24,25]. In addition, gephyrin plays a crucial role in synaptic dynamics and is a platform for multiple protein-protein interactions and bringing receptors. Thus, we examined the distribution of gephyrin as an indicator for functional GABA$_A$ receptors in amygdala[26]. In *Lis1*$^{+/+}$ mice, somata and proximal dendrites of amygdala neurons exhibited a variety of gephyrin clusters from very small round puncta to large and bright clusters (Fig. 5b). While *Lis1*$^{+/-}$ mice displayed similar pattern of gephyrin clusters with *Lis1*$^{+/+}$ mice, they were significantly decreased (Fig. 5b, e). Decreased gephyrin clusters in *Lis1*$^{+/-}$ mice were rescued by SNJ1945 treatment commencing at P10 (Fig. 5b, e). Thus, we concluded that post-natal treatment of SNJ1945 was effective for recovery of defective network formation and decreased receptor distribution in amygdala.

SNJ1945 augmented retrograde transport of nerve growth factor (NGF) in dorsal root ganglia (DRG) neurons. Neural growth
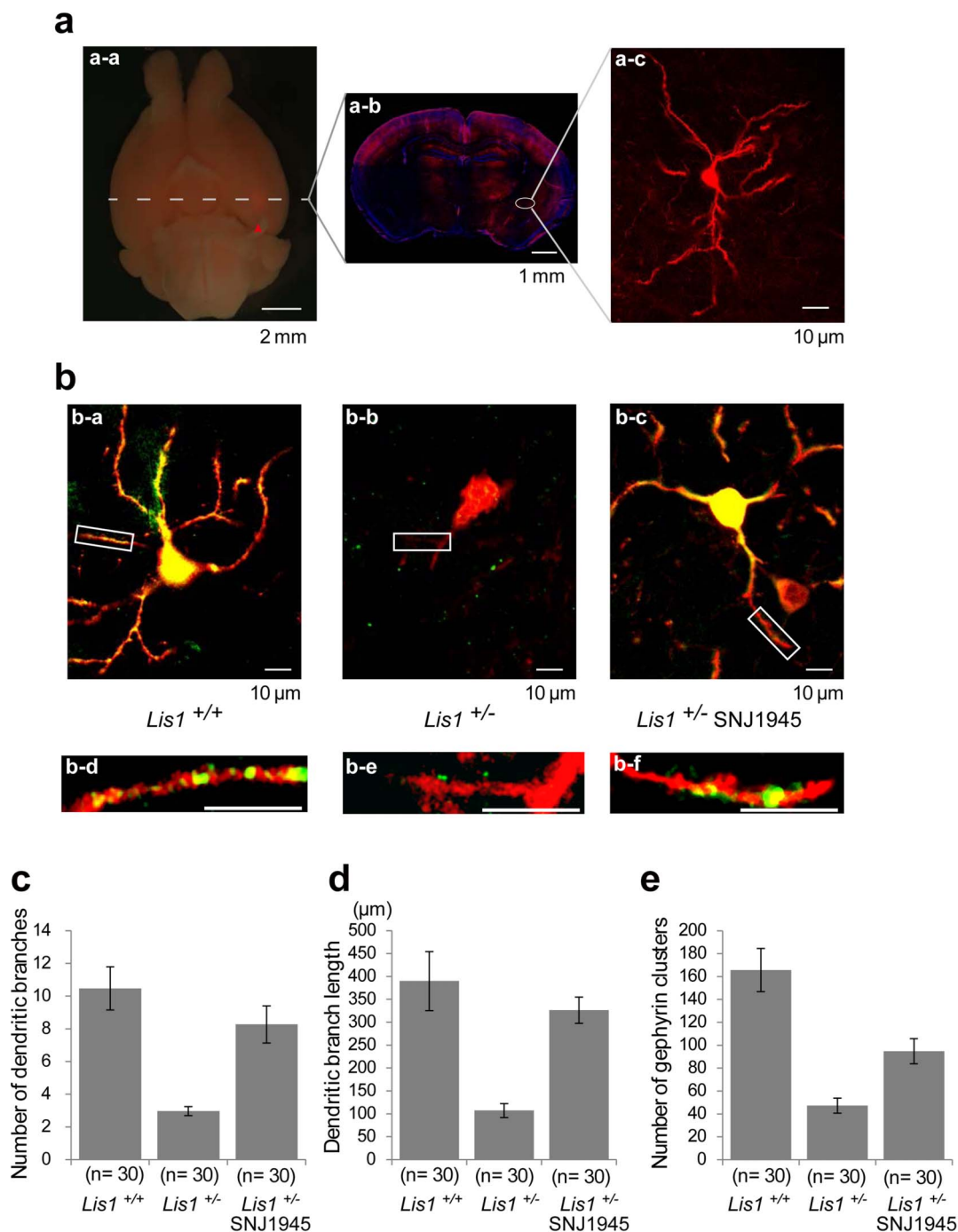
Figure 5 | Examination of neuronal networks and clustering of GABA receptors. (a) Neural fibers were visualized by the expression of TdTomato through *in utero* gene transfer. Ventral view image of whole brain by fluorescence dissecting microscope (a-a), confocal images at low (a-b) and high magnifications of representative fields (a-c) from coronal amygdala (white circle) are shown. (b) Individual image of amygdala neurons. Neural fiber was visualized by the TdTomato expression (red), which was decorated by gephyrin clusters (green). Representative images from *Lis1*^{+/+} mice (b-a, d), *Lis1*^{+/−} mice (b-b, e) and *Lis1*^{+/−} mice with P10 treatment (b-c, f) are shown. Note: *Lis1*^{+/−} mice exhibited poor arbors of neural fiber and decreased clusters of gephyrin, which were rescued by the treatment of SNJ1945. We examined five independent transfected brains for each, which were subjected to serial cryostat section with 5 μm thickness. Statistical examination of branching frequency (c), total length of branches (d) and number of gephyrin clusters (e) was performed.

factors are crucially important for activity-dependent plastic changes in synaptic strength and network refinement. We assumed that the SNJ1945 dependent rescue of neural network formation and receptor distribution might be attributable to the recovery of retrograde transport of neural growth factors. Retrograde axonal transport of nerve growth factor (NGF) signals is critical for the survival, differentiation, and maintenance of peripheral sympathetic and sensory neurons and basal forebrain cholinergic neurons. To examine retrograde transport of NGF, we used quantum dots (Qd-NGF) to track retrograde transport of NGF in cultures of mouse DRG neurons. Using pseudoTIRF microscopy, we tracked the movement of Qd-NGF in live DRG neurons in real time[27]. We applied non-compartmentalized cultures of DRG neurons, which displayed both directional movements of Qd-NGFs. Live-cell
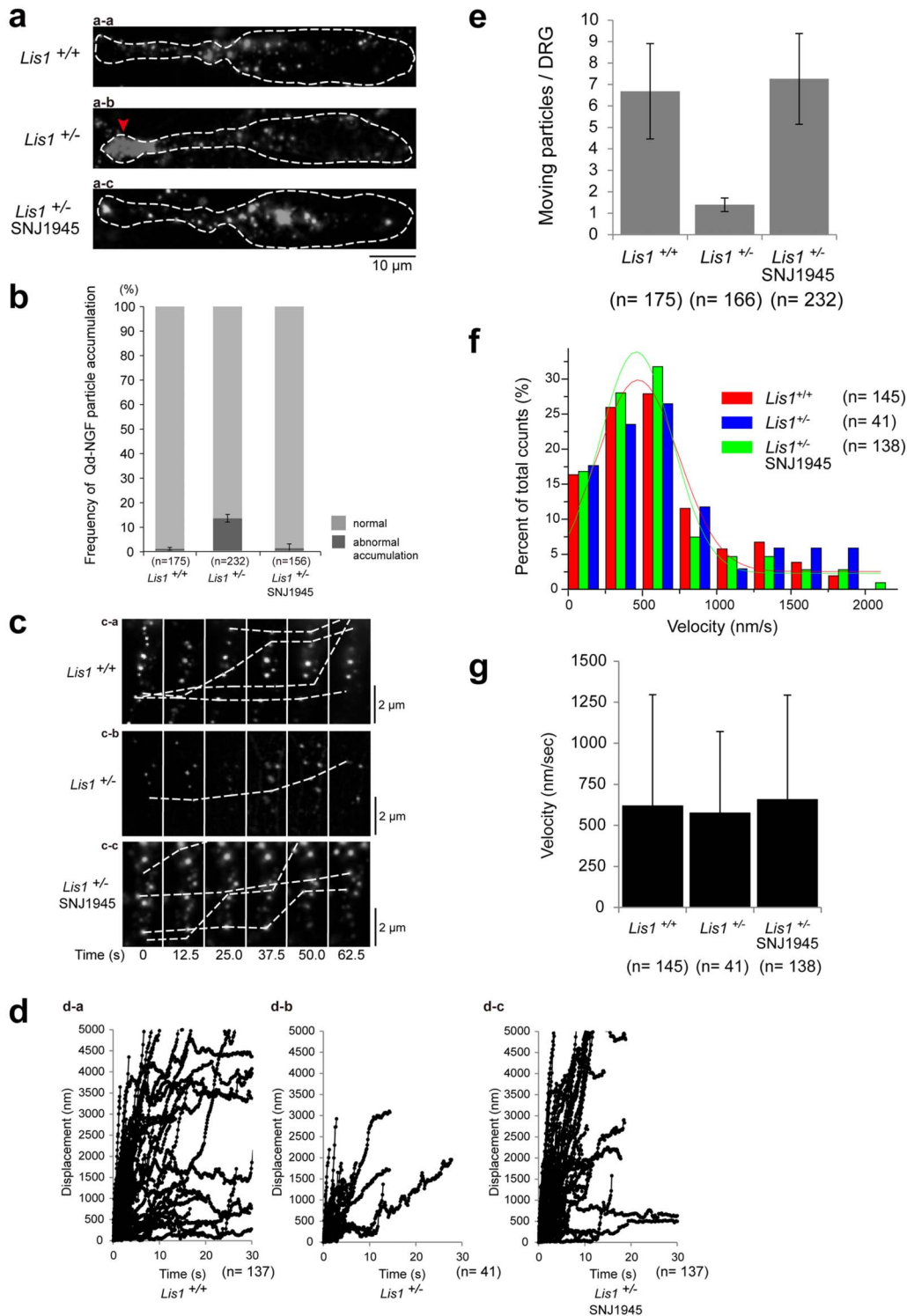
a

a-a
Lis1 $^{+/+}$

a-b
Lis1 $^{+/-}$

a-c
Lis1 $^{+/-}$
SNJ1945

10 µm

b

(%)
Frequency of Qd-NGF particle accumulation

100
90
80
70
60
50
40
30
20
10
0

(n=175)   (n=232)   (n=156)
Lis1 $^{+/+}$ *Lis1* $^{+/-}$ *Lis1* $^{+/-}$
SNJ1945

normal
abnormal
accumulation

c

c-a
Lis1 $^{+/+}$
2 µm

c-b
Lis1 $^{+/-}$
2 µm

c-c
Lis1 $^{+/-}$
SNJ1945
2 µm

Time (s)   0   12.5   25.0   37.5   50.0   62.5

d

d-a

5000
4500
4000
3500
3000
2500
2000
1500
1000
500
0
Displacement (nm)
0   10   20   30
Time (s)   (n= 137)
Lis1 $^{+/+}$

d-b

5000
4500
4000
3500
3000
2500
2000
1500
1000
500
0
Displacement (nm)
0   10   20   30
Time (s)   (n= 41)
Lis1 $^{+/-}$

d-c

5000
4500
4000
3500
3000
2500
2000
1500
1000
500
0
Displacement (nm)
0   10   20   30
Time (s)   (n= 137)
Lis1 $^{+/-}$
SNJ1945

e

10
9
8
7
6
5
4
3
2
1
0
Moving particles / DRG

Lis1 $^{+/+}$ *Lis1* $^{+/-}$ *Lis1* $^{+/-}$
SNJ1945
(n= 175) (n= 166) (n= 232)

f

Percent of total counts (%)

Lis1 $^{+/+}$ (n= 145)
Lis1 $^{+/-}$ (n= 41)
Lis1 $^{+/-}$ (n= 138)
SNJ1945

Velocity (nm/s)
0   500   1000   1500   2000

g

1500
1250
1000
750
500
250
0
Velocity (nm/sec)

Lis1 $^{+/+}$ *Lis1* $^{+/-}$ *Lis1* $^{+/-}$
SNJ1945
(n= 145) (n= 41) (n= 138)

Figure 6 | Retrograde transport of NGF in DRG neurons. To show that the Qd-NGF complex can be internalized at axon terminals and transported in a retrograde fashion to neuron cell bodies, quantum dots were conjugated to NGF (Qd-NGF) and incubated with DRG neurons followed by pseudoTIRF microscope examination. (a) Qd-NGF were internalized and transported to the cell body. White dotted line indicates the contour of DRG neurons. DRG neurons from *Lis1*$^{+/+}$ mice (a-a), *Lis1*$^{+/-}$ mice (a-b) and *Lis1*$^{+/-}$ mice with P10 treatment (a-c) are shown. Note: in *Lis1*$^{+/-}$ mice, Qd-NGF dots were internalized, but aberrantly accumulated at the tips of DRG neurons (red arrowhead). (b) Each percentage of abnormal accumulation was presented as mean ± SEM. n indicates the number of examined DRG neurons. Aberrant accumulation was exclusively observed in in *Lis1*$^{+/-}$ mice, which was rescued by SNJ1945 treatment. (c) Transport dynamics of Qd-NGF containing endosomes. Time-lapse video images of endosomes are shown. Lapsed time is shown at the bottom of panel. Retrograde transport of Qd-NGF containing endosomes in *Lis1*$^{+/-}$ mice was decreased (c-b). (d) Trajectories of endosomes from *Lis1*$^{+/+}$ mice (d-a), *Lis1*$^{+/-}$ mice (d-b) and *Lis1*$^{+/-}$ mice with P10 treatment (d-c) are shown. (e) Number of transported endosomes per DRG neuron was presented as mean ± SEM. n indicates the number of examined DRG neurons. Note: We found that significant reduction of the frequency in *Lis1*$^{+/-}$ mice, which was rescued by SNJ1945 treatment. (f) Histograms of velocities of retrograde-directed endosomes. (g) Mean velocities are 0.62 µm/s in *Lis1*$^{+/+}$ mice, 0.60 µm/s in *Lis1*$^{+/-}$ mice and 0.65 µm/s in *Lis1*$^{+/-}$ mice with P10 treatment. There was no significant difference in each group.

imaging revealed that Qd-NGFs were internalized at axon terminals and transported in a retrograde fashion to cell bodies in DRG neurons from *Lis1*^{+/+} mice (Supplementary movie 1). Importantly, Qd-NGFs were internalized, but accumulate aberrantly at tips of DRG neurons from *Lis1*^{+/−} mice (Fig. 6a, b). This aberrant accumulation was rescued by treatment of SNJ1945 (Fig. 6a, b). Our observations were similar with transport defects peroxisomes and endosomes in the genetic absence of *Lis1/nudF* of filamentous fungus *Aspergillus nidulans*[28]. Next, we characterized the transport of Qd-NGF containing endosomes. Kymographs from time-lapse videos of Qd-NGFs indicated that the retrograde transport of Qd-NGF containing endosomes moved in a stop-and-go manner (Fig. 6c, d, Supplementary movie 1). Strikingly, we found that the frequency of retrograde transport of Qd-NGF containing endosomes was significantly decreased in DRG neurons from *Lis1*^{+/−} mice (Fig. 6c, d, e, Supplementary movie 2), whereas the frequency of anterograde transport of Qd-NGF containing endosomes was not affected (Supplementary Fig. 9). In clear contrast, the velocity of retrograde transport of Qd-NGF containing endosomes was intact in DRG neurons from *Lis1*^{+/−} mice (Fig. 6f, g), which was also consistent with *Aspergillus nidulans*[28]. We next examined the effect of SNJ1945 in the decreased frequency of the retrograde transport. Importantly, the treatment of SNJ1945 clearly recovered the defective retrograde transport of Qd-NGF containing endosomes (Fig. 6c, d, e, Supplementary movie 3). Presumably, the protection of LIS1 degradation by SNJ1945 restored proper dynein distribution, resulting in the recovery of retrograde transport of Qd-NGF containing endosomes, which may stimulate network formation and receptor distribution.

Discussion

SNJ1945 is permeable to the BBB, and was effective in rescuing defects in *Lis1*^{+/−} mice after treatment commenced perinatally. These findings suggest that SNJ1945 may be considered for the treatment of lissencephaly patients postnatally. In support of this, we demonstrated that SNJ1945 improved behavioral performances and brain glucose metabolism after treatment ten days after birth without histological rescue of brain disorganization. We also demonstrated that SNJ1945 stimulated network formation and receptor distribution, explaining functional rescue by SNJ1945. These functional rescues are partially attributable to restoration of growth signal, characterized by the recovery of retrograde transport of Qd-NGF containing endosomes. These findings support a potential therapeutic approach with a novel calpain inhibitor, SNJ1945, in the human ILS patient that has a *LIS1* mutation.

Methods

BrdU birthdating and proliferation studies. All mouse experiments were performed under the approval from the experimental animal committee of Osaka City University Graduate School of Medicine or the approval of the experimental animal committee of Osaka City University Graduate School of Medicine, National Institute for Physiological Sciences and Fujita Health University.

For bromodeoxyuridine (BrdU) experiments, pregnant dams (E15.5) were injected with BrdU (50 μg/g, i.p.), and the distribution of BrdU-positive cells was determined at P5. For pulse labeling to examine proliferation of neuroepithelial stem cell, pregnant dams (E13.5) were injected with BrdU (150 μg/g, i.p.). Subsequently, the distribution of BrdU-positive cells was determined one hour after injection. The incorporation of BrdU in cells was detected with a mouse anti-BrdU monoclonal primary antibody (Roche) followed by an alkaline phosphatase-conjugated secondary antibody (Boehringer Mannheim). We analyzed three independent mice for each genotype.

Histological examination and immunohistochemistry. After perfusion with 4%PFA fixative, tissues from wild type and mutant mice were embedded in paraffin and sectioned at 5 μm thickness. After deparaffination, endogenous peroxidase activity was blocked by incubating the sections in 1.5% peroxide in methanol for 20 min. The sections were then boiled in 0.01 M/liter citrate buffer, pH 6.0, for 20 min and cooled slowly. Before staining, the sections were blocked with rodent block (LabVision) for 60 min. The sections were washed in PBS and incubated with an anti-Brn-1 antibody (Santa Cruz).

Cell culture and immunocytochemistry. Human fibroblasts were grown in D-MEM supplemented with 10% FBS. To inhibit calpain, cells were incubated with 200 μM SNJ1945 or control DMSO for 2 hrs. Cells were fixed in 4% PFA in PBS followed by permealization with 0.2% Triton X-100 in PBS. Coverslips were blocked for one hour with Block Ace (Yukijirushi) in PBS supplemented with 5% BSA, and were incubated for 1 hr in primary antibody, washed, and incubated for 1 hr using Alexa 546-conjugated secondary antibodies (Molecular Probes). Primary antibodies were an anti-βCOP antibody (Sigma) and an anti-DIC1 antibody (Chemicon).

Behavioral analysis. *Lis1*^{+/+} mice and *Lis1*^{+/−} mice that were treated with and without SNJ1945 were used for behavioral experiments, as described in the figure legend for Figure 2a. *Lis1*^{+/−} mice had a single *Lis1* mutant allele. In this study mice were on an FVB background. All behavioral tests were carried out with male mice that were at least 9 weeks old at the start of testing. Raw data from the behavioral tests, the date on which each experiment was performed, and the age of the mice at the time of the experiment are shown in the mouse phenotype database (http://www.mouse-phenotype.org/). Mice were group-housed (four mice per cage) in a room with a 12 h light/dark cycle (lights on at 7:00 a.m.) with access to food and water *ad libitum*. The room temperature was kept at 23 ± 2°C. Behavioral testing was performed between 9:00 a.m. and 6:00 p.m. After the tests, all apparatus were cleaned with diluted sodium hypochlorite solution to prevent a bias due to olfactory cues. Three independent groups of mice were prepared for behavioral tests. One group consisted of equal numbers of mice. *Lis1*^{+/+}; *Lis1*^{+/+} mice without treatment, *Lis1*^{+/−}; *Lis1*^{+/−} mice without treatment, *Lis1*^{+/−}E9.5; *Lis1*^{+/−} mice with oral administration from from E9.5 (200 μg/g) followed by oral administration after birth (200 μg/g), *Lis1*^{+/−}P0; *Lis1*^{+/−} mice with oral administration from peri-natal period (200 μg/g) *Lis1*^{+/−}P10; *Lis1*^{+/−} mice with oral administration from ten days after birth (200 μg/g). Experiments were done in the following sequences; the first group (12 each): the general health and neurological screen including wire hang test (GHNS), light/dark transition (LD), rotarod (RR) and gait analysis (GA); the second group (16 each): GHNS, LD, RR and GA; the third group (24 each): GHNS, LD, open field (OF), elevated plus maze (EP), hot plate (HP), one-chamber social interaction test (SI), RR, Crawley's sociability and preference for social novelty test (CSI), startle response/prepulse inhibition test (PPI), Porsolt forced swim test (PS), fear conditioning test (FZ), tail suspension test (TS), and social interaction test in home cage (HC-SI). Behavioral data were obtained automatically by applications based on the public domain Image J program and modified for each test by Tsuyoshi Miyakawa (available through O'HARA & CO., Tokyo, Japan)[29]. Each behavioral test was separated from each other at least by 1 day.

Briefly, the rotarod test, using an accelerating rotarod (UGO Basile Accelerating Rotarod), was performed by placing mice on rotating drums (3 cm diameter) and measuring the time each animal was able to maintain its balance on the rod. The speed of the rotarod accelerated from 4 to 40 rpm over a 5-min period. Gait analysis was performed using ventral plane videography as described. Mice were placed on the treadmill belt that moves at a speed of 24.7 cm/s. Digital video images of the underside of mice were collected at 150 frames per second. The paw area indicates the temporal placement of the paw relative to the treadmill belt. The color images were converted to their binary matrix equivalents, and the areas (in pixels) of the approaching or retreating paws relative to the belt and camera were calculated throughout each stride. Plotting the area of each digital paw print (paw contact area) imaged sequentially in time provides a dynamic gait signal, representing the temporal record of paw placement relative to the treadmill belt. For Porsolt forced swimming test, the apparatus consisted of four plastic cylinders (20 cm height × 10 cm diameter). The cylinders were filled with water (23°C) up to a height of 7.5 cm. Mice were placed into the cylinders, and their behavior recorded over a 10-min test period. Data acquisition and analysis were performed automatically, using Image PS software (see above). All behavioral testing procedures were approved by the Animal Care and Use Committee of National Institute for Physiological Sciences and Fujita Health University.

MicroPET scan and data analysis. PET imaging data were obtained in male mice (20–30 g) using a small animal PET camera (microPET Focus-220, Simens Medical Systems), which has a transaxial resolution of 1.4 mm in full width at half-maximum. Data were acquired in a 128 × 128 × 95 matrix with a pixel of 0.475 mm and a slice thickness of 0.796 mm. Before PET scanning, mice were intravenously injected with ^{18}F-FDG (approximately 0.5 MBq/g B.W.) through a cannula inserted into the tail vein and were kept in their home cage for 30 min for the ^{18}F-FDG uptake under freely moving condition. Subsequently, the mice were placed in the small-animal PET scanner under isoflurane anesthesia (4% for induction and 1.5% for maintenance) with O_2 and N_2O gas. Static acquisitions were performed during 30 min. PET images were reconstructed using a filtered backprojection (FBP) algorithm. The image data acquired from microPET were analyzed by ASIPro VM (ver. 6.0, Concorde Microsystems Inc.) and PMOD (ver. 3.4, PMOD Technologies Ltd.) software. The PET and magnetic resonance (MR) images were co-registered using a PMOD software. MR images were obtained from *Lis1*^{+/+} mice and *Lis1*^{+/−} mice used for the PET study under isoflurane anesthesia with a 7 tesla MR scanner (BioSpec 70/20, Bruker). Volumetric regions of interest were placed on the several brain regions (striatum, cerebral cortex, hippocampus, thalamus, cerebellum, hypothalamus, amygdala, basal forebrain and septum, brain stem, midbrain, superior colliculi) based on the MR images. Relative regional ^{18}F-FDG uptake was determined by normalized count data to those in the whole brain. Each value was presented as mean ± SEM. Statistical analysis was performed using the SPSS Statistics Student software. Data

were analyzed using one-way ANOVA followed by *post hoc* Tukey's test for comparison among groups. Significance threshold was assumed at P < 0.05.

In utero transfection. Expression vectors were introduced into fetal brains by an *in utero* electroporation-mediated gene transfer method[20]. Briefly, pregnant mice were deeply anesthetized at E16.5, and the uterine horns were exposed. Approximately 2 μl of *TdTomato* plasmid solution was injected into the lateral ventricle from outside the uteri with a glass micropipette (GD-1.5, Narishige, Tokyo, Japan). Each embryo in the uterus was then placed between the tweezers-type electrodes described above and electronic pulses (45 V; 50 msec duration) were applied five times at intervals of 950 msec (GUY21, Bexco ltd). The uterine horns were then placed back into the abdominal cavity to allow the embryos to continue normal development. Histological examination was performed 5 days after *in utero* injection (P2-P3). Histological examination was performed 35 days after *in utero* injection (P30). SNJ1045 as applied from P10 by oral administration.

Examination of retrograde transport of NGF by pseudoTIRF microscope and live imaging. NGF was conjugated with Qd655 via carboxyl group substitution by using the coupling reagent 1-ethyl-3-(3-dimethylaminopropyl) -carbodiimide (EDAC) (Pierce Biotech, Rockford, IL). An inverted microscope (Olympus 1 × 71) was modified for pseudoTIRF illumination. The laser beam (488 nm) was focused at the back focal plane of the objective lens (ApoN×60, 1.49 Oil, Olympus). The incident angle was adjusted to be slightly smaller than the critical angle so that the laser beam could penetrate ≈1 μm into the aqueous solution. To image transport of Qd-NGF in live neurons, DRG neurons were incubated with Qd-NGF. Fluorescence images were filtered with a Qd655/15 emission filter. Time-lapse images were acquired by using an EMCCD camera (ImageM, Hamamatsu photonics) at the speed of 5–10 frames per second.

LC-MS/MS analysis. The SNJ1945 concentration in the brain was determined by turbo ion spray on an API 4000 triple-quadrupole mass spectrometer (Applied Biosystems) equipped with a turbo ion spray source using multiple reaction monitoring (MRM). Chromatography was performed on a NANOSPACE SI-2 HPLC system (Shiseido) with Shiseido Capcell pak C18 MG-II column. The extraction of SNJ1945 from the brain and the measuring condition were described in the literature[9].

1. Beckmann, N. *et al.* In vivo mouse imaging and spectroscopy in drug discovery. *NMR Biomed* **20**, 154–185 (2007).
2. Reiner, O. *et al.* Isolation of a Miller-Dieker lissencephaly gene containing G protein beta-subunit-like repeats. *Nature* **364**, 717–721 (1993).
3. Hattori, M., Adachi, H., Tsujimoto, M., Arai, H. & Inoue, K. Miller-Dieker lissencephaly gene encodes a subunit of brain platelet-activating factor acetylhydrolase [corrected]. *Nature* **370**, 216–218 (1994).
4. Vallee, R. B., Tai, C. & Faulkner, N. E. LIS1: cellular function of a disease-causing gene. *Trends Cell Biol* **11**, 155–160 (2001).
5. Wynshaw-Boris, A. Lissencephaly and LIS1: insights into the molecular mechanisms of neuronal migration and development. *Clin Genet* **72**, 296–304 (2007).
6. Yamada, M. *et al.* LIS1 and NDEL1 coordinate the plus-end-directed transport of cytoplasmic dynein. *Embo J* **27**, 2471–2483 (2008).
7. Yamada, M. *et al.* Inhibition of calpain increases LIS1 expression and partially rescues in vivo phenotypes in a mouse model of lissencephaly. *Nat Med* **15**, 1202–1207 (2009).
8. Koumura, A. *et al.* A novel calpain inhibitor, ((1S)-1((((1S)-1-benzyl-3-cyclopropylamino-2,3-di-oxopropyl)carbonyl)-3-methylbutyl) carbamic acid 5-methoxy-3-oxapentyl ester, protects neuronal cells from cerebral ischemia-induced damage in mice. *Neuroscience* **157**, 309–318 (2008).
9. Shirasaki, Y., Yamaguchi, M. & Miyashita, H. Retinal penetration of calpain inhibitors in rats after oral administration. *J Ocul Pharmacol Ther* **22**, 417–424 (2006).
10. Oka, T. *et al.* Amelioration of retinal degeneration and proteolysis in acute ocular hypertensive rats by calpain inhibitor ((1S)-1-((((1S)-1-benzyl-3-cyclopropylamino-2,3-di-oxopropyl)amino)carbony l)-3-methylbutyl)carbamic acid 5-methoxy-3-oxapentyl ester. *Neuroscience* **141**, 2139–2145 (2006).
11. Sasaki, S. *et al.* Complete loss of Ndel1 results in neuronal migration defects and early embryonic lethality. *Mol Cell Biol* **25**, 7812–7827 (2005).
12. Hirotsune, S. *et al.* Graded reduction of Pafah1b1 (Lis1) activity results in neuronal migration defects and early embryonic lethality. *Nat Genet* **19**, 333–339 (1998).
13. Yingling, J. *et al.* Neuroepithelial stem cell proliferation requires LIS1 for precise spindle orientation and symmetric division. *Cell* **132**, 474–486 (2008).
14. McEvilly, R. J., de Diaz, M. O., Schonemann, M. D., Hooshmand, F. & Rosenfeld, M. G. Transcriptional regulation of cortical neuron migration by POU domain factors. *Science* **295**, 1528–1532 (2002).
15. Manent, J. B., Wang, Y., Chang, Y., Paramasivam, M. & LoTurco, J. J. Dcx reexpression reduces subcortical band heterotopia and seizure threshold in an animal model of neuronal migration disorder. *Nat Med* **15**, 84–90 (2009).
16. Paylor, R. *et al.* Impaired learning and motor behavior in heterozygous Pafah1b1 (Lis1) mutant mice. *Learn Mem* **6**, 521–537 (1999).
17. Mizuma, H., Shukuri, M., Hayashi, T., Watanabe, Y. & Onoe, H. Establishment of in vivo brain imaging method in conscious mice. *J Nucl Med* **51**, 1068–1075 (2010).
18. Pfund, Z. *et al.* Lissencephaly: fetal pattern of glucose metabolism on positron emission tomography? *Neurology* **55**, 1683–1688 (2000).
19. Palmer, A. E. & Tsien, R. Y. Measuring calcium signaling using genetically targetable fluorescent indicators. *Nat Protoc* **1**, 1057–1065 (2006).
20. Takitoh, T. *et al.* Activation of Aurora-A Is Essential for Neuronal Migration via Modulation of Microtubule Organization. *J Neurosci* **32**, 11050–11066 (2012).
21. Davis, M., Walker, D. L. & Myers, K. M. Role of the amygdala in fear extinction measured with potentiated startle. *Ann N Y Acad Sci* **985**, 218–232 (2003).
22. LeDoux, J. E. Emotion circuits in the brain. *Annu Rev Neurosci* **23**, 155–184 (2000).
23. Pare, D., Quirk, G. J. & Ledoux, J. E. New vistas on amygdala networks in conditioned fear. *J Neurophysiol* **92**, 1–9 (2004).
24. Takahashi, H. *et al.* Selective control of inhibitory synapse development by Slitrk3-PTPdelta trans-synaptic interaction. *Nat Neurosci* **15**, 389–398, S381–382 (2012).
25. van Versendaal, D. *et al.* Elimination of inhibitory synapses is a major component of adult ocular dominance plasticity. *Neuron* **74**, 374–383 (2012).
26. Chhatwal, J. P., Myers, K. M., Ressler, K. J. & Davis, M. Regulation of gephyrin and GABAA receptor binding within the amygdala after fear acquisition and extinction. *J Neurosci* **25**, 502–506 (2005).
27. Cui, B. *et al.* One at a time, live tracking of NGF axonal transport using quantum dots. *Proc Natl Acad Sci U S A* **104**, 13666–13671 (2007).
28. Egan, M. J., Tan, K. & Reck-Peterson, S. L. Lis1 is an initiation factor for dynein-driven organelle transport. *J Cell Biol* **197**, 971–982 (2012).
29. Yamasaki, N. *et al.* Alpha-CaMKII deficiency causes immature dentate gyrus, a novel candidate endophenotype of psychiatric disorders. *Mol Brain* **1**, 6 (2008).

Acknowledgements

Author contributions

S.H. performed mouse histological examination and mouse behavioral analyais. M.Y. performed mouse histological examination. K.T., S.H. and T.M. performed mouse behavioral analyais (Figure 3). Y.K. and Y.T. performed PET analysis (Figure 4). K.K., Y.O., H.W. and M.S. performed neural circuit characterization (Figure 5, 6). M.A. provided us SNJ1945. K.H., M.A., K.T. and M.K. provided us a fibroblast cell line from the human lissencephaly patient. A.W.-B. and S.H. organized experiments and wrote a manuscript.

Additional information

How to cite this article: Toba, S. *et al.* Post-natal treatment by a blood-brain-barrier permeable calpain inhibitor, SNJ1945 rescued defective function in lissencephaly. *Sci. Rep.* **3**, 1224; DOI:10.1038/srep01224 (2013).